IOP Publishing | The Japan Society of Fluid Mechanics Fluid *Dynamics* Research

Fluid Dyn. Res. **46** (2014) 061420 (12pp) doi:10.1088/0169-5983/46/6/061420

Circulation shedding in viscous starting flow past a flat plate

Monika Nitsche[1] **and Ling Xu**[2]

[1] Department of Mathematics and Statistics, Albuquerque, University of New Mexico, NM, USA
[2] Department of Applied and Computational Mathematics and Statistics, University of Notre Dame, Notre Dame, IN, USA

E-mail: nitsche@math.unm.edu and lxu6@nd.edu

Received 7 July 2014, revised 20 September 2014
Accepted for publication 1 October 2014
Published 13 November 2014

Communicated by Y Fukumoto

Abstract

Numerical simulations of viscous flow past a flat plate moving in the direction normal to itself reveal details of the vortical structure of the flow. At early times, most of the vorticity is attached to the plate. This paper introduces a definition of the shed circulation at all times and shows that it indeed represents vorticity that separates and remains separated from the plate. During a large initial time period, the shed circulation satisfies the scaling laws predicted for self-similar inviscid separation. Various contributions to the circulation shedding rate are presented. The results show that during this initial time period, viscous diffusion of vorticity out of the vortex is significant but appears to be independent of the value of the Reynolds number. At later times, the departure of the shed circulation from its large Reynolds number behaviour is significantly affected by diffusive loss of vorticity through the symmetry axis. A timescale is proposed that describes when the viscous loss through the axis becomes relevant. The simulations provide benchmark results to evaluate simpler separation models such as point vortex and vortex sheet models. A comparison with vortex sheet results is included.

1. Introduction

Flow past sharp corners leads to separation and roll-up of the boundary vorticity into a vortex, called the starting vortex. Detailed understanding of the starting flow is of intrinsic interest and is also important in many applications from engineering, biology, and physics. For example, the induced forces are relevant during flying or swimming (see, e.g., Wang 2000, Eldredge 2007). Details of the spiral roll-up, including an instability on the outer spiral turns,

have been visualized experimentally (e.g., Pierce 1961, Taneda and Honji 1971, Pullin and Perry 1980, Lian and Huang 1989, Lepage *et al* 2005). Asymptotic scaling laws for the spiral shape in self-similar inviscid flow were found by Pullin (1978). The goal of this paper is to find the shed circulation and associated shedding rates for viscous flow past a flat plate using well-resolved numerical simulations. Since at early times much of the vorticity is attached to the plate, it is not clear *a priori* how to define the separated vorticity. We propose a method to compute the shed circulation and use it to investigate its dependence on Reynolds numbers. We also investigate several viscous and inviscid contributions to the circulation shedding rate.

This work is motivated in part by low-order models used to simulate separated flows, such as point vortex models (Cortelezzi and Leonard 1993, Michelin and Llewellyn Smith 2009, Ysasi *et al* 2011) and vortex sheet models (Jones 2003, Alben 2010, Eldredge 2005). These models have the advantage of being significantly more computationally efficient than direct numerical simulations, and thus enable simulating the flows to large times. Comparison of the models with laboratory experiment (Nitsche and Krasny 1994) or direct numerical simulations (Eldredge and Wang 2010, Sheng *et al* 2012) shows agreement in large-scale features of the flow, but also reveals discrepancies in the shed circulation and induced forces. One goal of the present work is to provide benchmark results with which to evaluate the low-order models.

We consider flow past a finite flat plate of zero thickness that is impulsively started in the direction normal to itself. Most closely related numerical works include those of Koumoutsakos and Shiels (1996), who studied flow past a flat plate using a viscous vortex method, and Luchini and Tognaccini (2002), who computed flow past a semi-infinite flat plate in a self-similar reference frame. The present work complements these earlier works by providing details of the vortex structure at early times and addressing the shed circulation.

The paper is organized as follows. Section 2 describes the problem considered and the numerical method used to compute the flow. Section 3 presents the numerical results, including the vorticity evolution at fixed Reynolds number $\mathrm{Re} = 500$ (section 3.1), the definition and discussion of associated circulation and shedding rates (section 3.2), the dependence on Reynolds numbers for $\mathrm{Re} = 250, 500, 1000, 2000$ (section 3.3), and a comparison with vortex sheet results (section 3.4). The results are summarized in section 4.

2. Problem formulation

2.1. Problem description

A finite plate of length L and zero thickness is immersed in viscous fluid and impulsively started from zero velocity to a constant velocity $U > 0$ in the direction normal to itself. The flow is nondimensionalized using the plate length L as the characteristic length scale and U as the characteristic velocity, with Reynolds number $\mathrm{Re} = LU/\nu$, where ν is the kinematic fluid viscosity. The flow is assumed to be two-dimensional and is described in nondimensional Cartesian coordinates $\mathbf{x} = (x, y)$, and time t, with fluid velocity $\mathbf{u}(\mathbf{x}, t) = (u(\mathbf{x}, t), v(\mathbf{x}, t))$ and vorticity $\omega(\mathbf{x}, t)$. Computations are performed in a reference frame moving with the plate in which the plate is positioned horizontally on the x-axis, centered at the origin, and the far field flow points upwards. The flow is modelled by the incompressible Navier–Stokes equations with constant density and is assumed to remain symmetric about $x = 0$ at all times.

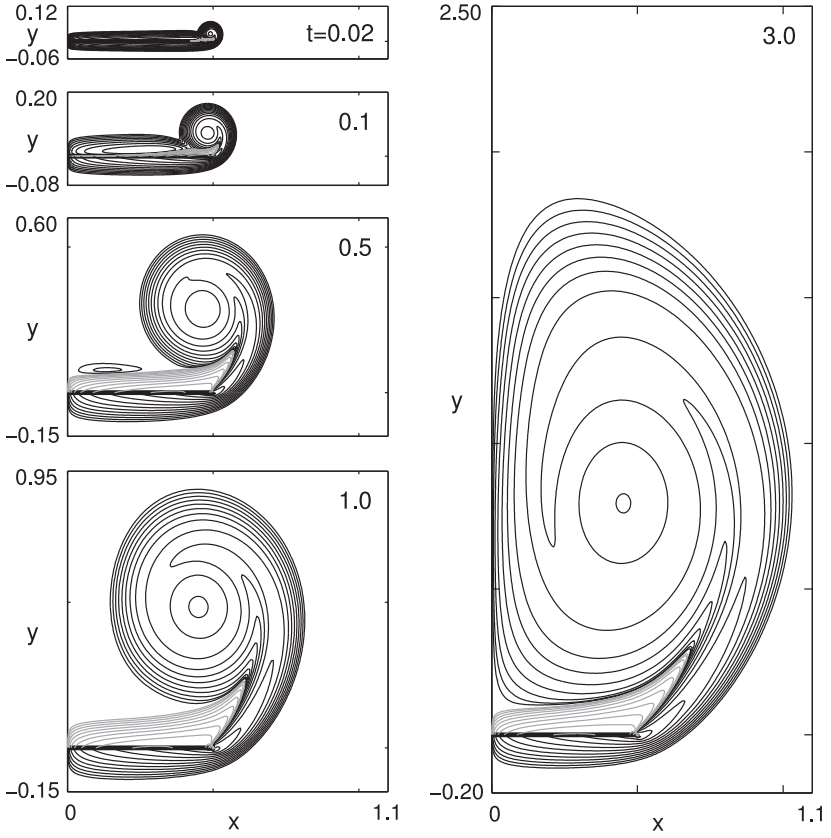

Figure 1. Vorticity for Re = 500, at a sequence of times $t = 0.02, 0.1, 0.5, 1.0, 3.0$, as indicated. The vorticity contour levels are $\omega = \pm 2^j$, $j = -5, \ldots, 12$.

2.2. Numerical method

The Navier–Stokes equations are solved in vorticity-streamfunction formulation using a finite-difference method on a regular grid, with semi-Lagrangian advection and time-splitting using uniform timesteps. The computational domain is a rectangular region in the right half plane, $x \geqslant 0$, that contains the plate. Boundary conditions on the plate are given by the no-slip condition. On the remaining open boundaries of the domain, the flow is specified by the potential flow induced by the far field and the interior vorticity. Initially, the interior vorticity is zero. The vorticity is updated in time using a time-splitting method. First, the interior vorticity is convected by a fourth-order semi-Lagrangian scheme. Then, the vorticity is diffused using an implicit fourth-order Crank–Nicholson method. The method was originally developed in Xu (2012) and is described in detail in Xu and Nitsche (2014a). For the present problem, in which the flow is highly singular near the tip of the plate, the method was found to converge to at least second order in space and first order in time. The spatial and temporal resolutions used are chosen so that the solution is well resolved and remains unchanged to the eye under further refinement. The results presented below were computed using a fine resolution of $\Delta x = 1/5120$, $\Delta t = 0.2 \times 10^{-5}$ for the smallest times and resolutions as coarse as $\Delta x = 1/160$, $\Delta t = 4 \times 10^{-4}$ for the larger times. The quantities plotted will be shown to be quite well resolved at all times.

3. Numerical results

3.1. Vorticity evolution, Re = 500

This section describes the computed vorticity evolution for a fixed value of Re = 500. Figure 1 shows the vorticity in the right half plane, at the indicated times. The vorticity contours are $\omega = \pm 2^j$, $j = -5, \ldots, 12$, with positive contours in black and negative contours in gray. The vorticity on the left half plane, not shown, is equal in magnitude but opposite in sign. We describe the evolution in the right half.

Initially, the background flow, which moves from bottom to top, induces positive horizontal velocity below the plate and negative horizontal velocity above. This generates a boundary layer of positive vorticity around the bottom and the top of the plate. The bottom vorticity is convected around the edge of the plate towards the top and immediately forms a concentrated region of vorticity. This vorticity, in turn, induces flow in a direction opposite to the background flow, thereby generating a small region of negative vorticity above the plate. This region, shown in gray, grows in time, together with the growing leading vortex. At later times, clearly seen here at $t \geqslant 0.5$, the negative vorticity is entrained into the leading vortex. It is noteworthy that in our computations, the generation of negative vorticity is already visible at time $t = O(\Delta t)$, within the first 10 timesteps, indicating that the negative vorticity region forms immediately after the start of the motion. This implies that the initial Rayleigh stage described by Luchini and Tognaccini (2002), in which the flow is potential everywhere except for a thin viscous boundary layer of constant thickness, is absent for impulsively started flow. Indeed, simulations of accelerated flows with plate velocities Ut^p show that the Rayleigh layer is present for $p > 0$ during an initial time interval, but that the length of this time interval shrinks to zero as $p \to 0$ (Xu and Nitsche 2014b).

We now describe the growth of the starting vortex arising from the boundary layer. Figure 1 shows that the positive vorticity in the leading vortex is initially connected to the positive boundary layer vorticity above the plate, as seen, for example, at $t = 0.02$, 0.1. However, the leading vortex entrains vorticity in a small neighbourhood of it, while vorticity outside this neighbourhood moves away from the vortex. As a result, the small region of positive vorticity connecting the boundary layer vorticity to the leading vortex becomes depleted, until, as at $t = 0.5$ shown here, the leading vorticity is completely separated from the positive boundary layer vorticity. After that, the positive boundary layer vorticity diffuses and has effectively disappeared at $t = 1.0$. The leading vortex continues to grow until its vorticity reaches the axis of symmetry, as seen here at $t = 3.0$. At later times, positive vorticity in the leading vortex leaves the associated region of recirculation and travels upstream.

3.2. Circulation and shedding rates, Re = 500

We are interested in computing the shed circulation. However, given the shown vorticity contours, it is not clear *a priori* how to define the 'separated vorticity.' The question is how to distinguish boundary layer vorticity from the vorticity in the leading vortex. In this section, we first define the region $\Omega(t)$ encircling the leading vortex that determines the shed circulation

$$\Gamma = \int_{\Omega(t)} \omega \, \mathrm{d}A. \tag{1}$$

We then show that the vorticity within Ω remains within, and thereby separate from, the boundary layer vorticity.

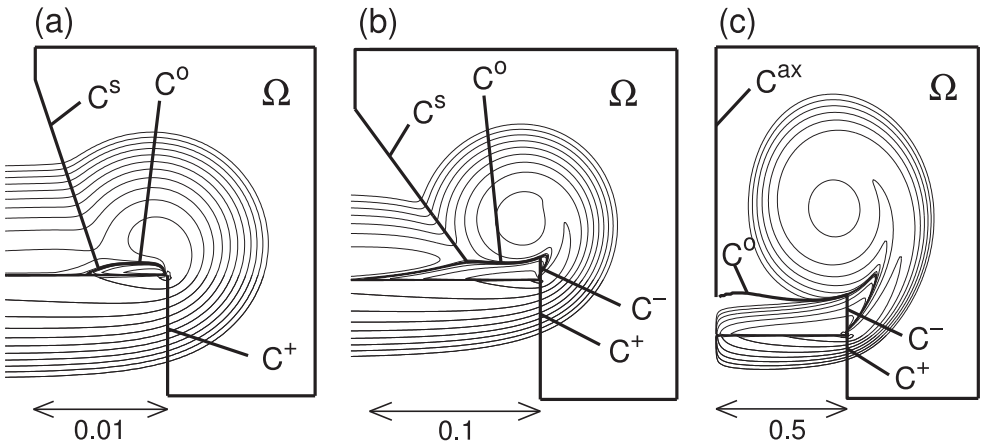

Figure 2. Sketch defining the domain Ω and portions C^+, C^-, C^s, C^o, C^{ax} of its boundary at (a) early times, (b) intermediate times, (c) late times. The approximate size of the vortex at these times is indicated by the arrows with the given lengths below the figures.

Figure 2 shows the definition of Ω in three different regimes in time. Figure 2(a) shows the vorticity at early times, here at $t = 0.0006$, at which the region of negative vorticity has not yet been entrained past the plate tip at $x = 0.5$. At these times, the region Ω is bounded below the plate by the vertical line through the tip, C^+. Above the plate it is bounded by the zero vorticity contour C^o and by a slanted line C^s through points of high curvature visible in the vorticity contours. That is, to define Ω we include all vorticity to the right of the tip, exclude the negative boundary layer vorticity, and limit the leading vortex on the left by the slant line. Figure 2(b) shows the vorticity at intermediate times, here at $t = 0.03$, when the negative vorticity above the plate has been entrained past $x = 0.5$. Here, we include all vorticity, positive or negative, to the right of $x = 0.5$, which introduces a small vertical piece of boundary C^- above the plate. The vorticity flux across C^- measures the amount of negative boundary layer vorticity that is entrained by the leading vortex. As will be described below, this component is also accounted for in the inviscid vortex sheet model. Figure 2(c) shows the vorticity at later times, here at $t = 1$, when all the positive boundary layer vorticity above the plate has diffused and effectively vanished. At this time the vortex is bounded on the left not by the slant line but by the axis C^{ax}. Each figure shows a typical length scale, indicating that the three regimes in time span three decades of length scales in space.

Figures 3(a) and (b) plot the shed circulation computed using the above definition, for fixed $\mathrm{Re} = 500$, on a linear and a logarithmic scale, for over four decades in time. The figures show results for six different meshsizes on six different time intervals. The data is an almost-continuous function of the meshsize, showing that the results are remarkably independent of the meshsize used in the computation. The logarithmic scale in figure 3(b) shows that the circulation satisfies the scaling behaviour predicted by inviscid similarity theory (Pullin 1978) surprisingly well,

$$\Gamma(t) \sim t^{1/3}\,, \tag{2}$$

during an initial time interval of approximately $t \leqslant 0.2$. The similarity theory holds for inviscid separation past a semi-infinite plate. In our case, at early times the vortex diameter is much less than the size of the plate, and the flow is comparable to that of viscous flow past a

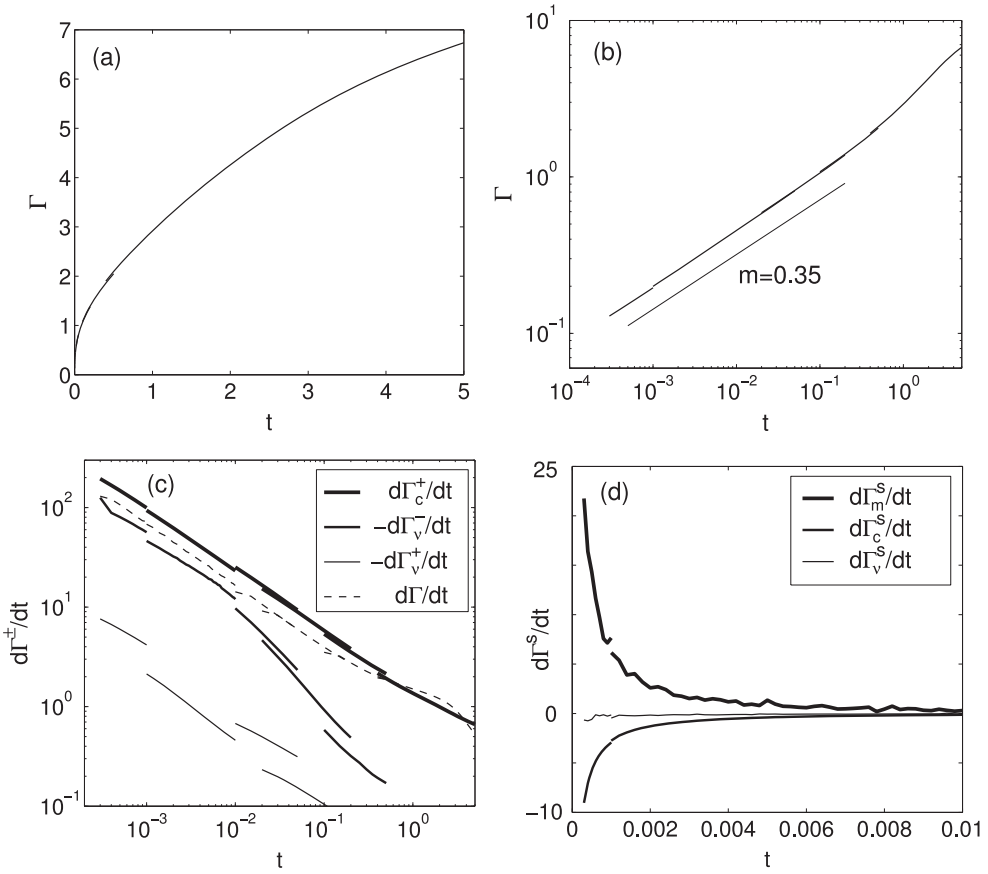

Figure 3. Circulation and shedding rates for Re = 500. (a), (b) Circulation $\Gamma(t)$. (c) Largest shedding rate components. (d) Shedding rates across C^s.

semi-infinite plate, which does not have an external length scale. Figure 3(b) indicates that around $t = 0.2$, about when the circulation reaches a value of one, the image vorticity introduced by the finite size of the plate becomes relevant and induces a deviation from the self-similar growth.

To determine the suitability of our definition of the shed circulation, and the effect of fluid viscosity, we investigate diffusive and convective contributions to the circulation shedding rate across different portions of the boundary $\partial\Omega$. From the Navier–Stokes equations and the transport and divergence theorems, we obtain

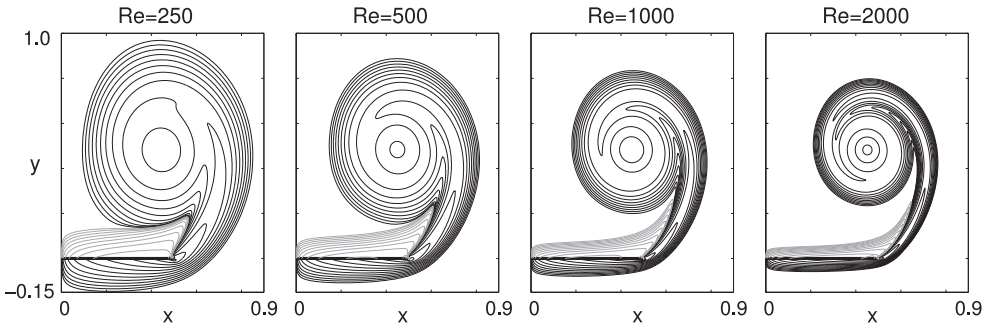

Figure 4. Vorticity at $t = 1$, with Re = 250, 500, 1000, 2000, as indicated. Contour levels are $\omega = \pm 2^j$, $j = -5, \ldots, 12$.

$$\begin{aligned}\frac{\mathrm{d}\Gamma}{\mathrm{d}t} &= \frac{\mathrm{d}}{\mathrm{d}t}\int_{\Omega(t)} \omega(\mathbf{x}, t)\mathrm{d}A = \int_{\Omega(t)} \frac{\partial\omega}{\partial t}\,\mathrm{d}A + \int_{\partial\Omega(t)} \omega(\mathbf{u}_{bd}\cdot\mathbf{n})\mathrm{d}s \\ &= \int_{\Omega(t)} \left[-(\mathbf{u}\cdot\nabla)\omega + \frac{1}{\mathrm{Re}}\Delta\omega\right]\mathrm{d}A + \int_{\partial\Omega(t)} \omega(\mathbf{u}_{bd}\cdot\mathbf{n})\mathrm{d}s \\ &= -\int_{\partial\Omega(t)} \omega\mathbf{u}\cdot\mathbf{n}\,\mathrm{d}s + \int_{\partial\Omega(t)} \frac{\nabla\omega}{\mathrm{Re}}\cdot\mathbf{n}\,\mathrm{d}s + \int_{\partial\Omega(t)} \omega(\mathbf{u}_{bd}\cdot\mathbf{n})\mathrm{d}s \\ &= \frac{\mathrm{d}\Gamma_c}{\mathrm{d}t} + \frac{\mathrm{d}\Gamma_\nu}{\mathrm{d}t} + \frac{\mathrm{d}\Gamma_m}{\mathrm{d}t}, \end{aligned} \tag{3}$$

where $\mathbf{n}$ is the outward normal and $\mathbf{u}_{bd}$ is the velocity of the boundary. Equation (3) defines the components of the vorticity flux due to convection, viscous diffusion, and the moving boundary, denoted by subscripts c, ν, and m, respectively. Notice that the only moving boundary portions defined in figure 2 are C^o and C^s, and only the latter has nonzero vorticity moving with it or convecting through it. Similarly, there is no convection of vorticity through C^{ax}. Thus, the only nonzero contributions to $\mathrm{d}\Gamma/\mathrm{d}t$ from the different boundary portions are the nine components

$$\frac{\mathrm{d}\Gamma_c^+}{\mathrm{d}t},\quad \frac{\mathrm{d}\Gamma_c^-}{\mathrm{d}t},\quad \frac{\mathrm{d}\Gamma_c^s}{\mathrm{d}t},\quad \frac{\mathrm{d}\Gamma_\nu^+}{\mathrm{d}t},\quad \frac{\mathrm{d}\Gamma_\nu^-}{\mathrm{d}t},\quad \frac{\mathrm{d}\Gamma_\nu^o}{\mathrm{d}t},\quad \frac{\mathrm{d}\Gamma_\nu^s}{\mathrm{d}t},\quad \frac{\mathrm{d}\Gamma_\nu^{ax}}{\mathrm{d}t},\quad \frac{\mathrm{d}\Gamma_m^s}{\mathrm{d}t},$$

where the superscript refers to the portion of the boundary and the subscript refers to the component of the shedding rate. For conciseness, we combine two of the viscous components into one:

$$\frac{\mathrm{d}\Gamma_\nu^-}{\mathrm{d}t} + \frac{\mathrm{d}\Gamma_\nu^o}{\mathrm{d}t} \to \frac{\mathrm{d}\Gamma_\nu^-}{\mathrm{d}t}.$$

Figures 3(c) and (d) show several of these components. The largest flux into Ω is the convective component through the vertical C^+ below the plate, $\mathrm{d}\Gamma_c^+/\mathrm{d}t$, shown in figure 3(c) as a thick curve. It is larger than $\mathrm{d}\Gamma/\mathrm{d}t$, which is shown as a dashed curve. The diffusive flux components are negative, with vorticity diffusing out of Ω, and reduce the total circulation. Of these, largest in magnitude is the diffusive flux through $C^- \cup C^o$, $\mathrm{d}\Gamma_\nu^-/\mathrm{d}t$. We conclude that $\mathrm{d}\Gamma_c^+/\mathrm{d}t$ is most significant, but the contribution to the total flux due to viscosity is nonnegligible, already at the earliest times computed.

Figure 3(d) shows the three nonzero flux components through the slant line. Note, first, that these are much smaller than the largest components shown in figure 3(c) and do not contribute significantly to the circulation, and second, that they vanish quickly and are

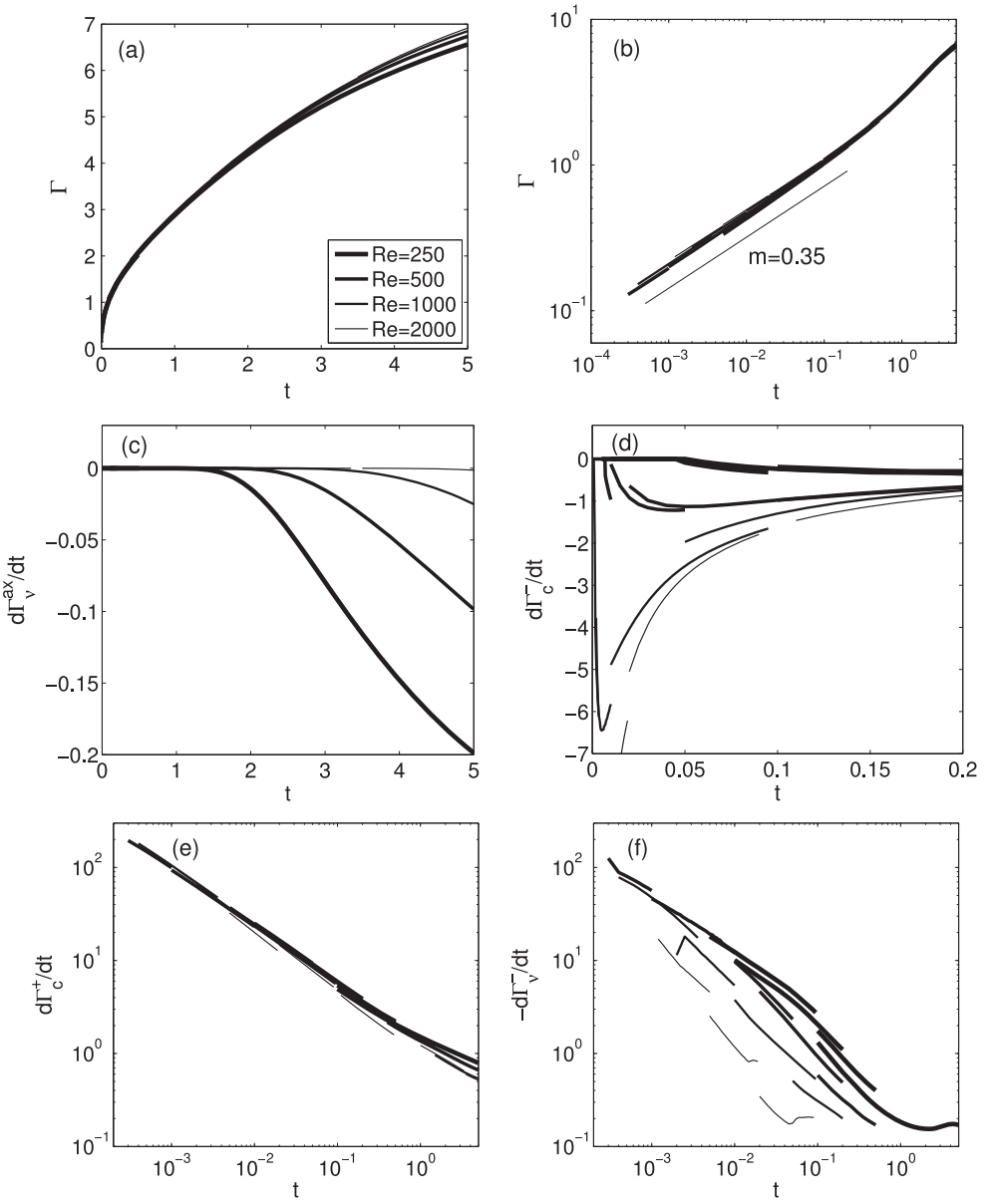

Figure 5. Circulation and shedding rates for Re = 250, 500, 1000, 2000. (a), (b) $\Gamma(t)$, (c) $\mathrm{d}\Gamma_\nu^{ax}(t)/\mathrm{d}t$, (d) $\mathrm{d}\Gamma_c^-(t)/\mathrm{d}t$, (e) $\mathrm{d}\Gamma_c^+(t)/\mathrm{d}t$, (f) $\mathrm{d}\Gamma_\nu^-(t)/\mathrm{d}t$.

negligibly small after about $t = 0.005$. Thus, not much vorticity leaves or enters through the slant line, making it a reasonable left boundary to the leading vortex.

3.3. Dependence on Re

Here, we investigate the dependence of the flow on Re based on results for Re = 250, 500, 1000, 2000. Figure 4 plots the corresponding vorticity contours at $t = 1$. As

Re increases, the vorticity maximum in the center of the vortex increases, the shear layers in the shed vorticity become thinner and stronger, and the overall vortical region shrinks, as does the boundary layer thickness.

Figure 5 plots the circulation and several circulation shedding components for this range of Re. Figure 5(a) shows that over most of the time interval shown, the circulation is practically independent of Re. Only at larger times is a deviation from the large Re behaviour noticeable, with circulation decreasing slightly as Re decreases. In the logarithmic scale shown in figure 5(b), no differences in Re are visible, and, in particular, the time at which the circulation departs from the self-similar inviscid scaling is independent of Re. We note that in the relatively large initial regime of self-similar growth, our results are consistent with viscous flow past a semi-infinite plate. In that case, Luchini and Tognaccini (2002) showed that, under an appropriate rescaling of length and time, the flow is independent of Re. Using their rescaling, our present results in the initial time period collapse to Reynolds-number-independent results (Xu and Nitsche 2014a).

Figure 5(c–f) plot several circulation flux components for the given Reynolds numbers. Figure 5(c) shows that the diffusion of vorticity through the axis, $\mathrm{d}\Gamma_\nu^{ax}/\mathrm{d}t$, which clearly depends on Re, is initially absent and increases as time increases. Figure 5(d) plots the convective entrainment of negative vorticity through the vertical C^- above the plate. It decreases sharply initially, then increases slowly to zero. Figure 5(e) plots the largest flux component, the convection of positive vorticity into the vortex through C^+, below the plate. This component is well resolved and clearly independent of Re. Figure 5(f) plots the next-largest component, the diffusive component $\mathrm{d}\Gamma_\nu^-/\mathrm{d}t$. It also appears to be independent of Re at early times, based on the results for $\mathrm{Re} = 250, 500, 1000$. The results at later times, and those for $\mathrm{Re} = 2000$, are not fully resolved, due to the difficulty in resolving the large vorticity gradients present near the tip of the plate.

We conclude from figure 5 that the circulation $\Gamma(t)$ and, consistent with it, the dominant flux components are essentially independent of Re during the times in which Γ grows self-similarly. The fact that the loss of vorticity due to viscous diffusion is significant during these times but largely independent on Re indicates that as Re increases, vorticity gradients increase but are offset by the factor $\frac{1}{\mathrm{Re}}$ in the diffusive term of equation (3),

$$\frac{1}{\mathrm{Re}} \int \nabla\omega \cdot \mathbf{n}\, \mathrm{d}s, \tag{4}$$

in such a way that the quotient remains approximately constant.

During the time of self-similar growth, the behaviour of all shedding rates is consistent with that for the semi-infinite plate flow, and $\Gamma(t)$ is close to Reynolds number independent. A closeup shows that small Re-dependent changes in Γ, proportional to its current value, grow slowly in time. These are small changes introduced by the finite plate length. At later times, the loss of vorticity through the axis, measured by $\mathrm{d}\Gamma_\nu^{ax}/\mathrm{d}t$, becomes significant and has a large effect on the total circulation. A measure of the time at which this component becomes relevant is given by the time t_ϵ^{ax} at which $|\mathrm{d}\Gamma_\nu^{ax}/\mathrm{d}t| = \epsilon$. Using $\epsilon = 0.001$, we obtain $t_\epsilon^{ax} = 1.41, 2.14, 3.18, 4.88$ for $\mathrm{Re} = 250, 500, 1000, 2000$, respectively, which closely satisfies $t_\epsilon^{ax} = 0.05 \cdot \mathrm{Re}^{0.6}$. Note that even when the flow is close to Re-independent, the viscous component of the circulation shedding rate remains significant.

3.4. Comparison with vortex sheet simulations

To conclude this paper, we present a brief comparison between the viscous flow and inviscid vortex sheet simulations. The inviscid model consists of approximating the separated vorticity

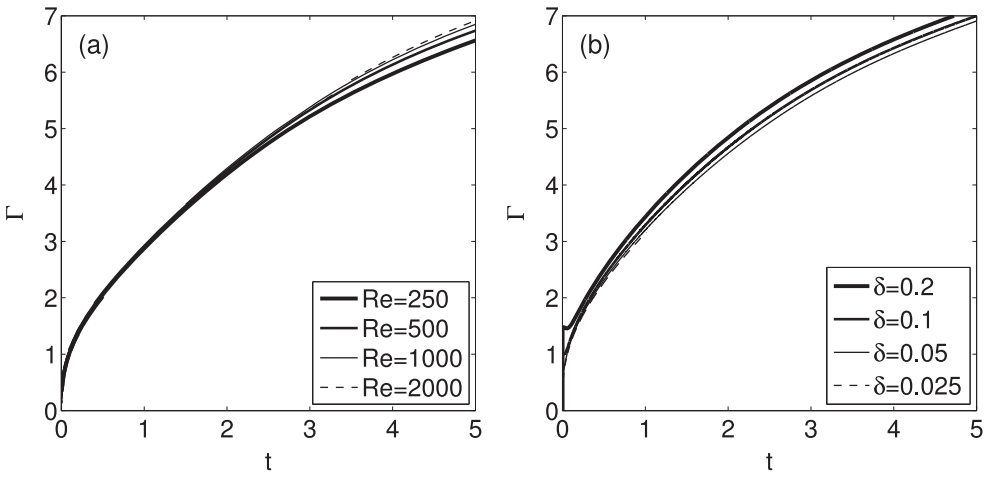

Figure 6. Shed circulation. (a) Viscous flow, for Re = 250, 500, 1000, 2000, as indicated. (b) Vortex sheet flow, for $\delta = 0.2, 0.1, 0.05, 0.025$, as indicated.

by a free vortex sheet, and the plate by a bound vortex sheet whose strength is determined such that the velocity normal to the walls vanishes. At time $t = 0^+$, only the bound sheet is present, and the induced potential flow is identical to the initial flow in the viscous case. At $t > 0$, the vortex sheet does not model boundary layers and is expected to approximate the viscous flow only in an outer region away from the wall vorticity. Boundary layer separation is modelled by a separating free vortex sheet, which is computed by releasing a point vortex from the plate tip at each timestep. The vortex has circulation determined from the Kutta condition,

$$\frac{\mathrm{d}\Gamma}{\mathrm{d}t} = \frac{1}{2}\left(u_+^2 - u_-^2\right), \tag{5}$$

and velocity parallel to the plate with magnitude

$$\bar{u} = \frac{1}{2}(u_+ + u_-)\,. \tag{6}$$

Here, u_+ and u_- are the tangential velocities at the tip below and above the plate, obtained from the vortex sheet strength and the average fluid velocity at the tip. Thus, the circulation shedding model includes a positive contribution from below the plate, and a negative contribution from above. One question of interest, although beyond the scope of this paper, is whether the model predicts the flux of negative vorticity through C^-, shown in figure 5(d). The free sheet is regularized using the vortex blob method, which consists of introducing a regularization parameter δ into the governing equations. We follow the details given in Nitsche and Krasny (1994).

Ideally, the vortex sheet simulations approximate high Reynolds number flow for sufficiently small values of δ. To determine the extent of the agreement, figure 6 compares the viscous flow circulation computed with an increasing sequence of Re = 250, 500, 1000, 2000 (figure 6(a)), with the vortex sheet circulation computed with a decreasing sequence of $\delta = 0.2, 0.1, 0.05, 0.025$ (figure 6(b)). As δ decreases, the total circulation decreases slightly. As Re increases, the total circulation increases. The apparent limiting values at the final time plotted, $t = 5$, are surprisingly close.

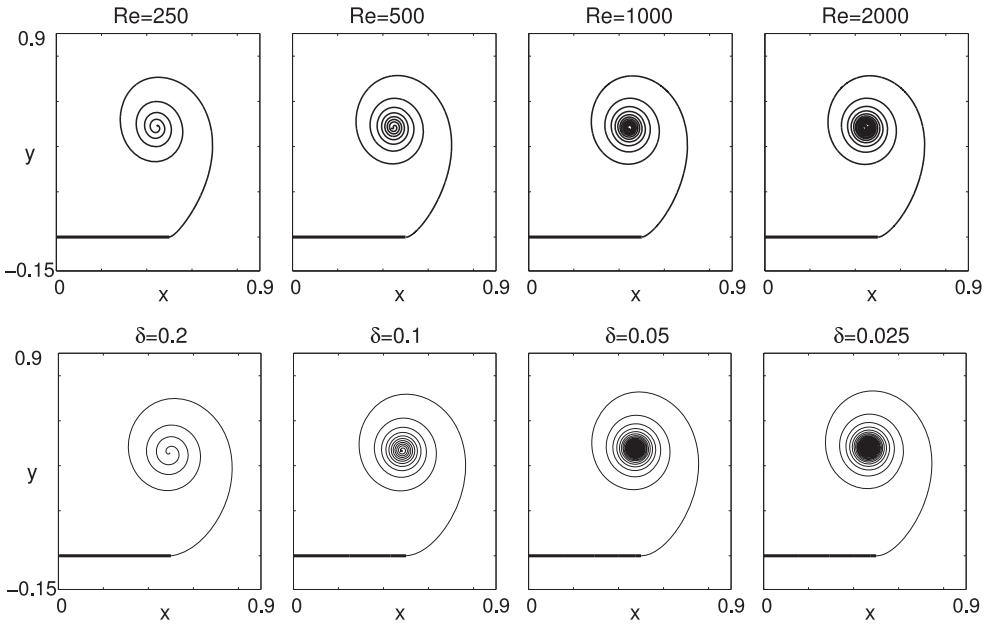

Figure 7. Streaklines at $t = 1$ of particles released at the tip of the plate, moving with the viscous flow at Re = 250, 500, 1000, 2000, as indicated (top row), and with the vortex sheet flow, computed with $\delta = 0.2, 0.1, 0.05, 0.025$, as indicated (bottom row).

Figure 7 compares streaklines in the viscous flow (top row) and the vortex sheet flow (bottom row), using the same sequence of Re and δ. The streaklines are obtained in each case by releasing particles at the tip of the plate at each timestep that move with the fluid velocity. In both cases, the streakline rolls up into a spiral, with overall agreement in spiral size and center position. In both cases, the roll-up becomes tighter, with more spiral turns, as Re increases and δ decreases, respectively. Differences are visible in the shape of the spiral roll-up. In the viscous flow, the spiral is more elongated, but in the vortex sheet flow, it is broader. Lepage *et al* (2005) reports similar results in comparisons of vortex sheet simulations with laboratory experiments. The differences decrease slightly as δ decreases.

4. Summary

Viscous flow past a flat plate that is impulsively started in the direction normal to itself is computed using a method based on fourth-order finite difference approximations and semi-Lagrangian advection for a range of Re = 250, 500, 1000, 2000. We compute the shed circulation as well as circulation shedding rates across various components of the boundary of the leading vortex. We find the following:

- The shed circulation satisfies self-similar scaling laws over more than three decades in time and is consistent with viscous flow past a semi-infinite plate. The circulation at these early times is basically independent on Re. Around $t = 0.2$, the lengthscale introduced by the plate causes a large deviation from self-similar growth.
- The two largest components of the circulation shedding rates are convection of vorticity into the leading vortex from below the plate and diffusion of vorticity out of the vortex

above the plate, near the tip. The diffusive component is significant, but it is also largely independent of the value of Re at early times.

- The deviation from high Re flow at larger times is significantly affected by diffusion of vorticity across the axis at late times, a component that can be computed accurately. This observation suggests a timescale t_ϵ^{ax} at which loss of vorticity through the axis becomes relevant.
- The shed circulation computed with the vortex sheet model is in good agreement with the viscous simulations.

References

Alben S 2010 Passive and active bodies in vortex-street wakes *J. Fluid Mech.* **642** 92–125

Cortelezzi L and Leonard A 1993 Point vortex model of the unsteady separated flow past a semi-infinite plate with transverse motion *Fluid Dyn. Res.* **11** 264–95

Eldredge J D 2005 Efficient tools for the simulation of flapping wing flows *AIAA* **2005-0085** 1–11

Eldredge J D 2007 Numerical simulation of the fluid dynamics of 2D rigid body motion with the vortex particle method *J. Comput. Phys.* **221** 626–48

Eldredge J D and Wang C 2010 High-fidelity simulations and low-order modeling of a rapidly pitching plate *AIAA* 2010–4281

Jones M 2003 The separated flow of an inviscid fluid around a moving flat plate *J. Fluid Mech.* **496** 405–41

Koumoutsakos P and Shiels D 1996 Simulation of the viscous flow normal to an impulsively started and uniformly accelerated flat plate *J. Fluid Mech.* **328** 177–226

Lepage C, Leweke T and Verga A 2005 Spiral shear layers: roll-up and incipient instability *Phys. Fluids* **17** 031705

Lian Q X and Huang Z 1989 Starting flow and structure of the starting vortex behind bluff bodies with sharp edges *Exp. Fluids* **8** 95–103

Luchini P and Tognaccini R 2002 The start-up vortex issuing from a semi-infinite flat plate *J. Fluid Mech.* **455** 175–93

Michelin S and Llewellyn Smith S G 2009 An unsteady point vortex method for coupled fluid-solid problems *Theor. Comput. Fluid Dyn.* **23** 127–53

Nitsche M and Krasny R R 1994 A numerical study of vortex ring formation at the edge of a circular tube *J. Fluid Mech.* **276** 139–61

Pierce D 1961 Photographic evidence of the formation and growth of vorticity behind plates accelerated from rest in still air *J. Fluid Mech.* **11** 460–4

Pullin D I 1978 The large-scale structure of unsteady self-similar rolled-up vortex sheets *J. Fluid Mech.* **88** 401–30

Pullin D I and Perry A E 1980 Some flow visualization experiments on the starting vortex *J. Fluid Mech.* **97** 239–55

Sheng J X, Ysasi A, Kolomenskiy D, Kanso E, Nitsche M and Schneider K 2012 Simulating vortex wakes of flapping plates *Natural Locomotion in Fluids and on Surfaces* (*The IMA Volumes in Mathematics and its Applications* vol 155) pp 255–62

Taneda S and Honji H 1971 Unsteady flow past a flat plate normal to the direction of motion *J. Phys. Soc. Jpn.* **30** 262–72

Wang Z J 2000 Vortex shedding and frequency selection in flapping flight *J. Fluid Mech.* **410** 323–41

Ysasi A, Kanso E and Newton P K 2011 Wake structure of a deformable Joukowski airfoil *Fluid Dynamics: From Theory to Experiment* **240** 1574–82

Xu L 2012 Viscous flow past flat plates *PhD Thesis* University of New Mexico

Xu L and Nitsche M 2014 Scaling behaviour in impulsively started viscous flow past a finite flat plate *J. Fluid Mech.* **756** 689–715

Xu L and Nitsche M 2014 Start-up flow past an accelerated flat plate, submitted, arXiv:1404.4585 [physics.flu-dyn]